Flexible piezo-capacitive pressure sensor for measurement of wind speed and direction

Ramanathan, Arun, Headings, Leon, Dapino, Marcelo

Arun K. Ramanathan, Leon M. Headings, Marcelo J. Dapino, "Flexible piezo-capacitive pressure sensor for measurement of wind speed and direction," Proc. SPIE 12046, Sensors and Smart Structures Technologies for Civil, Mechanical, and Aerospace Systems 2022, 1204607 (18 April 2022); doi: 10.1117/12.2614329

SPIE.

Event: SPIE Smart Structures + Nondestructive Evaluation, 2022, Long Beach, California, United States

Flexible piezo-capacitive pressure sensor for measurement of wind speed and direction

Arun K. Ramanathan, Leon M. Headings, and Marcelo J. Dapino

NSF IUCRC on Smart Vehicle Concepts, Department of Mechanical and Aerospace Engineering, The Ohio State University, Columbus, OH 43210

ABSTRACT

Demand for autonomous flying vehicles intended for transportation of people and goods is expected to accelerate in the next few years as urban air mobility maturity reaches level-4, a rating implying that hundreds of flights will simultaneously take off from urban aerodromes around the country. Wind sensors available on the vehicles and located in the air space will become a key necessity for ensuring safe navigation. Conventional anemometers suffer from various drawbacks due to their non-aerodynamic construction, high power consumption, complex signal processing, and cost. An airfoil-shaped low drag anemometer is presented for wind speed and direction measurement on tethered systems such as kites, balloons, and drones. The airfoil anemometer is equipped with a flexible, dual-layer capacitive pressure sensor with a polyvinylidene fluoride (PVDF) diaphragm for wind speed and a commercial digital magnetometer for wind direction measurement. The fabrication process for the diaphragm-type capacitive sensor is presented, along with characterization of the sensor in a pressure chamber. The completed sensor is then integrated into a NACA-2412 profile airfoil, along with a commercial magnetometer, for demonstration in a laboratory-scale wind tunnel.

Keywords: Anemometer, wind pressure and direction sensing, capacitive sensor, PVDF, airfoil

1. INTRODUCTION

A sensor system detecting wind speed and direction plays a critical role in airborne tethered applications, such as kites, balloons, and drones, for precise control, trajectory optimization, and monitoring the environment. In addition, wind speed measurements serve as inputs in the wind energy sector for energy forecasting and to optimize the performance of wind turbines [1]. Airplanes and unmanned aerial systems typically use pitot tubes to measure airspeed. Pitot tubes are vulnerable to icing, necessitating anti-icing electrical heaters to prevent blockages. The electrical heaters reduce the energy efficiency of small and micro-aerial vehicles. There is also an increasing demand for accurate, low-cost wind monitors that are both scalable and efficient [2].

Cup and vane anemometers are the most common instrument for measuring wind speed and direction [2, 3]. They are installed primarily in weather observatories and wind farms and are considered a reliable instrument for surveying wind conditions. In spite of their structural robustness, they are typically large, heavy, and induce a large amount of drag, thus making them unsuitable for aerial applications. In addition, they suffer from high rotational inertia and friction between the components, making them unsuitable for measuring rapid changes such as wind gusts. Heated-element or thermal anemometers measure wind speed and direction through measurement of the heat loss and/or temperature distribution induced by airflow [4]. There are two types of thermal anemometers - calorimetric and hot wire. In the calorimetric type, the wind speed and direction are determined by the temperature gradient measured by the various sensing elements within the device. On the other hand, the hot-wire type is a thermistor that measures the change in resistance due to the heat lost in an airflow. A bridge circuit measures the variation in resistance that is calibrated against the wind speed. The primary advantages of this technology are its high accuracy and small footprint. However, in both techniques, the active element needs to be continuously heated which results in high power consumption for remote sensing

Further author information: (Send correspondence to M.J.D.)
A.K.R.: E-mail: ramanathan.38@osu.edu
V.S.C.: E-mail: headings.4@osu.com
M.J.D.: E-mail: dapino.1@osu.edu

Sensors and Smart Structures Technologies for Civil, Mechanical, and Aerospace Systems 2022, edited by Daniele Zonta, Branko Glisic, Zhongqing Su, Proc. of SPIE Vol. 12046, 1204607 · © 2022 SPIE · 0277-786X · doi: 10.1117/12.2614329

Table 1: Features of different anemometer technologies.

	Rotating	Heated-element	Acoustic	Drag
Wind speed measurement principle	Periodic establishment of electrical contact	Flow induced temperature change	Time-of-flight	Defomation due to differential pressure, vortex shedding
Wind direction measurement principle	Wind vane	Thermal gradient	Differential response of sensors along sonic axes	Differential response of sensors in an array
Active materials	Switches, potentiometers, triboelectrics, etc.	Heaters and thermometers	Piezoelectric transducers	Piezoresistive, piezoelectric, optical, etc.
Advantages	High accuracy, structural robustness	High accuracy, small footprint	No moving parts, good dynamic response	Small footprint, low power consumption, and low cost
Disadvantages	Large and heavy, moving parts, poor dynamics	Temperature drift, high power consumption, low range of measurement	Size, complex signal processing, complex fabrication process, temperature effects	Temperature dependency, low range of measurements, relatively low accuracy

relying on batteries or harvested energy. They also suffer from temperature drift and rapid thermal fluctuations at turbulent wind speeds [5, 6].

There are also methods that utilize ultrasonic transducers to measure wind speed based on transit-time calculations [7]. Ultrasonic anemometers use high-frequency vibrating membranes functioning as both transmitter and receiver of acoustic waves. Wind speed is obtained using the time-difference between the transmitted and received pulses [8]. In order to measure wind direction in addition to wind speed, more than two transceivers are utilized and their relative difference in the time-of-flight or the phase difference between the transmitted and received signals is utilized to compute the wind direction. The configuration in which ultrasonic transducers are arranged within the anemometer leads to a non-aerodynamic design resulting in high aerodynamic drag.

Drag anemometers involve deflection of an active material when subjected to an airflow. The deflection is then measured using piezoelectric [9], piezoresistive [10], or optical-based [11] strain gages. In spite of their small size, lower power consumption, and lower cost, it is challenging to arrange these sensors around a tether to obtain reliable wind direction measurements. Also, applicability of these sensors to a larger range of wind speed measurements needs further investigation. Table 1 summarizes the features of the anemometer technologies described above.

2. AIRFOIL ANEMOMETER

This paper presents an airfoil-shaped, low-drag anemometer as part of a smart tether system as illustrated in Figure 1. The smart tether system consists of several airfoil-shaped smart sleeves that not only reduce the overall drag on the system, but also perform sensing, actuation, and energy harvesting functions to control, optimize, and autonomize the airborne system. An airfoil profile can provide up to 10 times lower aerodynamic drag than a circular cross-section with an equal frontal area [12]. Each airfoil along the length of the tether can rotate freely or could be equipped with high torsional compliance to ensure its alignment with the direction of the wind to maximize drag reduction and increase the efficiency of the tethered airborne system.

One of the desired functionality of the tethered airfoil is to simultaneously monitor the wind conditions, namely wind speed and direction, at a given altitude. It has been observed empirically and analytically, that

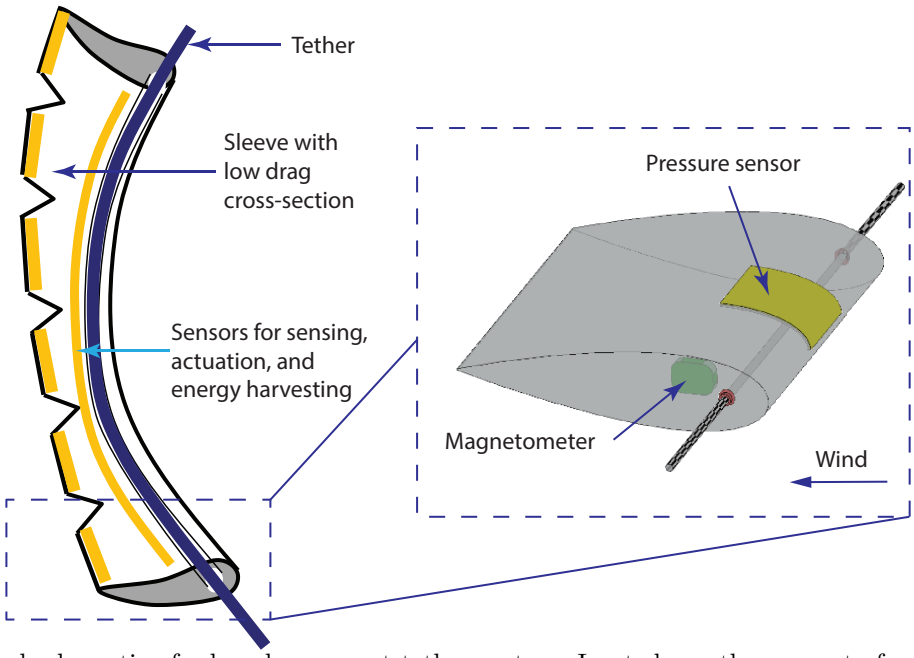

Figure 1: Notional schematic of a low-drag, smart tether system. Inset shows the concept of an airfoil-shaped anemometer instrumented with a conformable pressure sensor and a magnetometer for wind speed and direction measurements, respectively.

at low wind speeds, when the tether is positioned at the center of pressure (approximately 1/4th of the chord length) of an airfoil, the magnitude of the aerodynamic moment generated by the surface pressure along the length of the airfoil remains constant [13] and aligns the airfoil to a constant angle-of-attack. The angle-of-attack is the angle formed by the chord of the airfoil and the direction of the wind. In other words, the airfoil acts as a wind vane and undergoes a structural motion to align itself in the direction of the wind at a unique and stable angle-of-attack. Thus, wind direction relative to a fixed reference can be obtained by measuring the structural motion of the airfoil. There are several suitable candidates to track the structural motion, such as angular encoders [14], potentiometers [15], and triboelectric devices [2]. However, these technologies rely on contact or friction between two surfaces and require engineered tribological interfaces to reduce the minimum wind speed at which direction can be measured. Further, potentiometer-based wind vanes, though robust and simpler in construction, consume high power and impede system autonomy and efficiency. To avoid measurements based on the relative motion of components, the motion of the airfoil can be tracked using a non-contact sensor such as a 3D digital magnetometer compass, which measures the change in earth's magnetic field intensity and measures absolute orientation of the airfoil relative to earth's magnetic north [16]. It also consumes relatively low power (less than 0.1 mW) and has a low operating voltage, making it suitable for powering via energy harvesters. However, it should be noted that the magnetic field of earth is a weak signal with a range of 0.5 to 0.65 Gauss and the precision of the magnetometer thus depends upon the inbuilt tilt compensation, environment, exposure to ferromagnetic materials in the proximity, and calibration procedure [16].

Once the airfoil has aligned itself in the direction of the wind, the surface pressure at any given point along the length of the airfoil at a constant angle-of-attack is directly proportional to the square of the wind velocity [17]. Due to the high resolution, conformability, and customization required for wind speed measurements, capacitive sensing technology is chosen over piezoelectric and piezoresistive techniques owing to its immunity to temperature changes, design flexibility, ease of fabrication, low cost, and low power consumption. The change in capacitance measured by the conformable capacitive pressure senor can be directly related to the wind speed using analytical models or calibration charts generated using reference anemometers. In the future, the airfoil is expected to be equipped with wind energy harvesters to harvest electrical energy from flow-induced vibrations to improve system autonomy [18].

3. FLEXIBLE CAPACITIVE PRESSURE SENSOR FOR WIND SPEED MEASUREMENTS

For an anemometer application, a pressure sensor with the following characteristics is desired: conformable to airfoil surface, relatively immune to temperature changes, ability to distinguish positive and negative pressures, possess high sensitivity and resolution to measure low wind pressures, low energy consumption, and ease of fabrication.

The surface pressure p at any given point on the airfoil at a given angle-of-attack is

$$p = \frac{1}{2} C_P \rho U^2, \tag{1}$$

where C_P is the profile-dependent coefficient of pressure at a given angle-of-attack, ρ is the air density, and U is the free-stream wind speed [17]. The above expression assumes the free-stream pressure to be equal to atmospheric pressure. A positive C_P value corresponds to compressive pressure on the airfoil surface, whereas a negative value corresponds to suction or lift. The above relationship can be utilized to measure wind speed U in terms of the applied pressure on the surface of the airfoil at its stable angle-of-attack as

$$U = \sqrt{\frac{2p}{\rho C_P}}. \tag{2}$$

So, for a maximum wind speed of about 18 m/s that can be achieved by the laboratory-scale wind tunnel, the maximum pressure on a NACA-2412 airfoil surface is expected to be below 350 Pa. However, to prevent shorting due to electrostatic forces, the sensor is designed for a maximum operating pressure of 500 Pa. The quadratic relationship also indicates requirement of a high accuracy sensing technology that is also relatively immune to temperature changes in airborne applications. Due to these demanding requirements, capacitive sensing is chosen as the most suitable candidate over a piezoelectric polyvinylidene fluoride (PVDF) sensor operating in the near-static sensing regime. Flexible capacitive sensors are also attractive due to their tunable pressure sensitivity, low electrical noise, and low power consumption [19, 20, 21].

In its most basic construction, a capacitive sensor consists of two conductive electrodes separated by a dielectric medium. An interrogating electric field penetrates through the dielectric material resulting in charges stored between the electrodes of the sensor [22]. Application of an external structural load alters the geometry of the displaced electric field resulting in changes in the displaced electric field that can be tracked as a change in the capacitance. Because the geometric changes in the capacitor are dependent on the applied load, the measured change in capacitance can be related to the applied load. Several configurations of capacitive sensors, such as multi-layered rectangular array [23], inter-digitated [24], and concentric ring-shaped [25] designs are available for measurement of mechanical loads. However, taking into consideration design flexibility, fabrication feasibility, and ease of integration onto a curved surface, a parallel-plate capacitive sensor is preferred for wind sensing applications.

A parallel-plate capacitor consists of two electrode layers separated by a dielectric medium. The capacitance C of a parallel-plate capacitor is given by

$$C = \frac{\varepsilon_0 \varepsilon_r A}{t}, \tag{3}$$

where ε_0 is permittivity of free space, ε_r is the relative dielectric constant of the medium, A is the common surface area between the two electrodes, and t is the thickness of the dielectric medium. As wind pressure is applied on the sensor, one of the electrodes deflect or deform and the thickness of the dielectric medium changes, resulting in a change in capacitance which is then related to the applied pressure. The change in capacitance ΔC of a parallel-plate capacitive sensor due to the applied pressure is given by

$$\Delta C(p) = \varepsilon_0 \varepsilon_r \left(\frac{A(0) + \Delta A(p)}{t(0) + \Delta t(p)} - \frac{A(0)}{t(0)} \right), \tag{4}$$

where $\Delta A(p)$ and $\Delta t(p)$ are the change in area of the electrode and thickness of the dielectric layer, respectively, due to the applied pressure p. Parameters $A(0)$ and $t(0)$ are the undeformed electrode area and thickness of the dielectric layer, respectively.

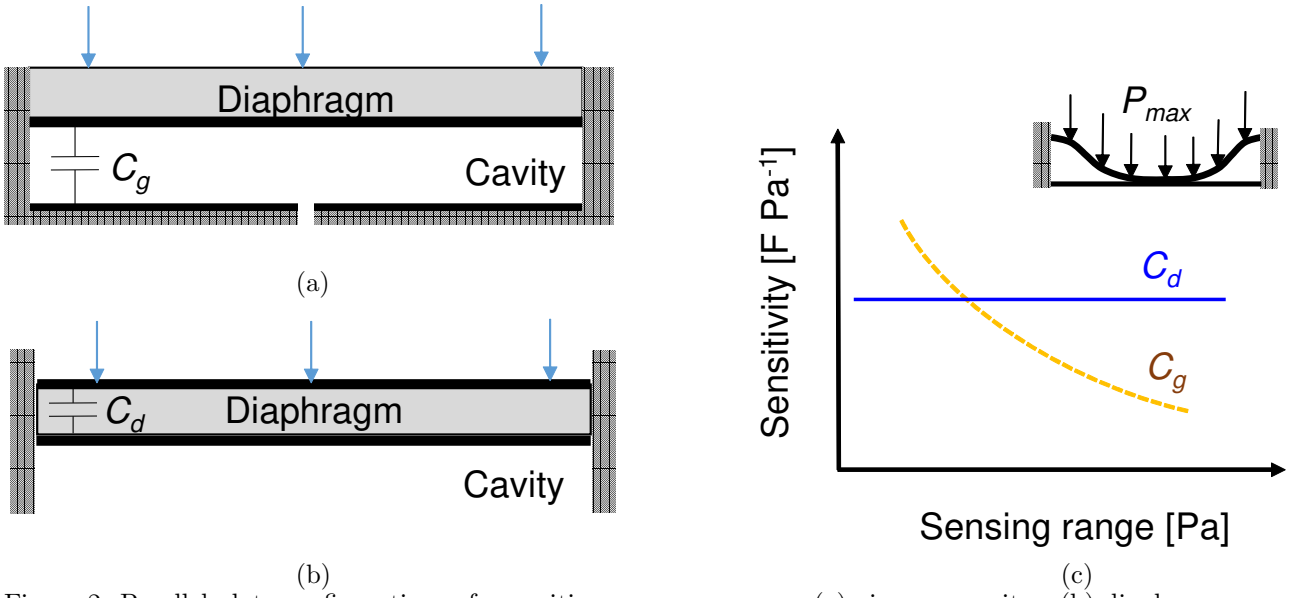

Figure 2: Parallel-plate configurations of capacitive pressure sensors: (a) airgap capacitor, (b) diaphragm capacitor, and (c) notional relationship between saturating sensing range and average pressure sensitivity of the airgap capacitor (yellow dashed line) and the diaphragm capacitor (blue solid line). The inset shows the deflection profile of the diaphragm at the maximum pressure measurable by the airgap capacitive sensor.

A parallel-plate capacitor can be realized in two different configurations as shown in Figure 2(a) and (b). The first configuration, shown in Figure 2(a), involves two conductive electrodes, one of them on a diaphragm, separated by air. When subjected to a compressive wind pressure, the diaphragm deflects toward the other electrode, resulting in a decrease in the airgap thickness and an increase in capacitance. The main advantage of this configuration is its ability to distinguish positive and negative pressures. The saturating sensing range, defined as the maximum pressure at which the two electrodes come into contact with each other, depends on the initial airgap. Since the average pressure sensitivity of the capacitive sensor depends on the initial airgap, an inverse relationship exists between the average pressure sensitivity and saturating sensing range as shown in Figure 2(c).

In the second configuration, shown in Figure 2(b), the diaphragm itself serves as a dielectric medium. When subjected to a wind pressure, the diaphragm layer stretches in-plane and due to Poisson's effect also causes a reduction in its thickness, resulting in an increase in capacitance. In comparison to the first configuration, the sensing range of the capacitive sensor is limited only by the yield strength of the diaphragm material. Further, the response of this capacitive sensor demonstrates better linearity in comparison to the airgap capacitor. In addition, high dielectric constant materials with large compliance [26], including PVDF, can be utilized for this configuration to increase its sensitivity and flexibility. Since the diaphragm always undergoes an in-plane extension irrespective of whether the applied pressure is positive or negative, this configuration cannot distinguish positive and negative pressures. Based on these considerations, we chose to investigate a dual layered circular capacitive sensor as shown in Figure 3 for wind pressure sensing applications in order to derive advantages from both configurations.

4. FABRICATION OF THE CAPACITIVE PRESSURE SENSOR

A non-lithographic approach is taken for construction of the flexible capacitive pressure sensor for wind speed monitoring. Therefore, the materials and their geometry are chosen based on commercial availability, ease of fabrication, and cost effectiveness. A 40 μm thick PVDF film is chosen as the diaphragm material due to its favorable structural properties, commercial availability with pre-sputtered silver electrodes, and high relative permittivity ($\varepsilon_r > 10$). Further, poled PVDF film serves as a piezoelectric material and offers opportunities for measuring dynamic pressure as well as energy harvesting applications. The radius of the diaphragm film is

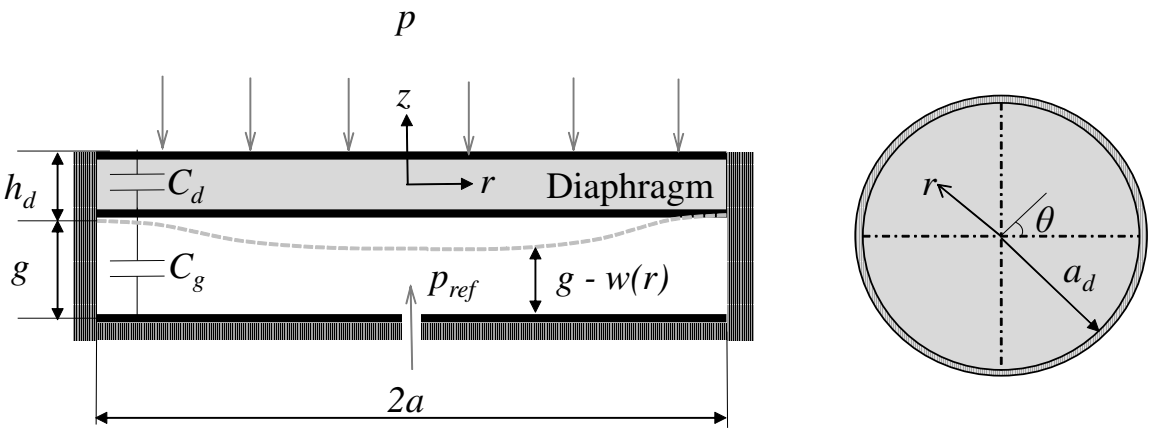

(a) (b)

Figure 3: Schematic of the dual layer circular capacitive sensor: (a) cross-sectional view and (b) top view.

chosen to be 9 mm based on the design of the final airfoil. Based on the above three design parameters, i.e., the diaphragm radius a, thickness of the diaphragm h_d, and elastic compliance of the diaphragm s_d, the initial airgap is determined to be 304 μm (or 12 mil) for a maximum operating pressure of 500 Pa for a laboratory-scale wind tunnel. Owing to its commercial availability, relatively low elastic modulus, and high insulation resistance (> 1 TΩ), Mylar is chosen for the base (I), insulation (II), and protection (III) layers. A schematic of the capacitive pressure sensor based on the chosen design parameters provided in Table 2 is shown in Figure 4(a).

To fabricate the sensor, a 25 μm thick copper foil with adhesive backing is attached to a 100 μm thick Mylar

Table 2: Geometric and material properties of the capacitive pressure sensor shown in Figure 4(b).

Dimensions		Material properties	
Parameter	Value	Parameter	Value
Diameter (a)	18 [mm]	Elastic modulus of diaphragm (E_d)	2 - 4 [GPa]
Designed airgap (g)	304 [μm]	Poisson's ratio of diaphragm (ν_d)	0.35
Thickness of diaphragm layer (h_d)	40 [μm]	Elastic modulus of Mylar sheet	4 - 6 [GPa]
Overall length x overall width	40 x 30 [mm x mm]	Relative dielectric constant of PVDF film (ε_r)	12

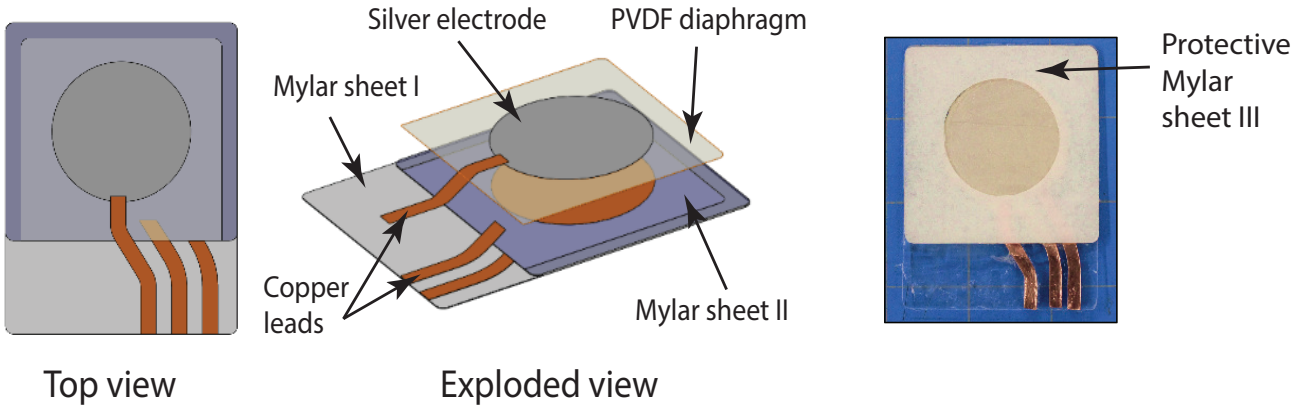

(a) (b)

Figure 4: (a) Schematic of the capacitive pressure sensor and (b) photograph of the actual sensor.

sheet (I). A circular shaped copper electrode is then cut out using a programmable precision cutter/plotter (Cameo Silhouette) to create the bottom electrode. The insulation layer consists of five sheets: two 127 μm thick Mylar sheets that are sandwiched between three 25 μm thick double sided adhesive tape sheets, yielding a total thickness of 329 μm. A circular cavity of diameter 18 mm is removed from this insulation layer using the precision cutter. The cavity is then aligned with the bottom copper electrode and attached to the bottom Mylar sheet using the double-sided adhesive tape. A border frame with the same thickness as the insulation layer is also created to guide alignment between the circular cavity and the bottom electrode. A small gap is provided between the insulation layer and the border, which is later filled with silicone to completely seal the air cavity after attaching the diaphragm. A shaped copper lead is then cut out and attached to the top of this insulation layer. This copper lead serves as the electrode for the diaphragm layer. A PVDF film with sputtered silver electrodes on both sides is cut to the dimensions 25 mm x 25 mm. Adhesive tape is attached to both sides of the PVDF film and circular masks are scored out using the precision cutter. After removing the scored regions on the adhesive tape, the excess silver electrodes are etched away and the circular masks are removed. The PVDF film is then attached to the copper leads using conductive epoxy and at other areas using a silicone-based flexible adhesive (Loctite) and cured at 65°C for 30 minutes. After curing for 24 hours, a 100 μm thick Mylar sheet (III) is then attached to the top surface to ensure clamping of the diaphragm layer. A photograph of the fabricated capacitive pressure sensor is shown in Figure 4(b). The overall dimensions of this capacitive sensor are 40 mm x 30 mm with a total thickness of only 0.54 mm. The sensor demonstrates good flexibility to conform with an airfoil structure. The low cost fabrication using commercially available materials, design flexibility, low profile, and multi-modal behavior of this flexible capacitive sensor make it an attractive candidate for other aerodynamic applications that require scalability and distributed sensing.

5. SENSOR CHARACTERIZATION IN A PRESSURE CHAMBER

A pressure measurement system is built to ensure suitability of the capacitive pressure sensor for integration with an airfoil for wind tunnel testing and to calibrate the measured change in capacitance with the applied pressure. A photograph of the experimental setup is shown in Figure 5(a). The system consists of a sealed pressure chamber with the capacitive pressure sensor attached to the top wall and with an air inlet and outlet. The inlet is connected to an inline check valve then a syringe pump for applying a desired static pressure to the sealed chamber. The piston of the syringe pump is attached to a threaded rod which is used to precisely adjust its stroke. The outlet of the sealed chamber is connected to a manometer (Rupse HT-1890). The sealed chamber is equipped with electrical leads that connect the capacitive pressure sensor to an LCR meter (B&K Precision 880). The LCR meter is connected to a Labview interface to record the capacitance data in the time-domain.

The capacitive pressure sensor is tested from -350 Pa to 350 Pa, based on the expected pressure on the airfoil in wind tunnel tests. The following tests are conducted in succession to characterize the capacitive pressure sensor: (i) measurement of change in air gap capacitance C_g with applied pressure under sealed cavity condition and (ii) measurement of change in diaphragm capacitance C_d with applied pressure under sealed cavity condition. After the above tests, a small hole is drilled on the top chamber wall and base (upper surface, opposite the diaphram as illustrated) of the capacitive sensor, as shown in Figure 5(b). The above tests (i) and (ii) are repeated with the cavity open to atmospheric pressure p_{atm}. Each of the above tests are repeated three times to ensure repeatability of the sensor readings.

Figure 6(a) shows the mean values of the changes in capacitance obtained from the four tests outlined above. It can be clearly seen that the sensor exhibits very low sensitivity for the sealed cavity compared to the open cavity. This is due to the fact that when the diaphragm deflects into the cavity, the cavity volume reduces and thus results in an increase in the cavity pressure. This increased cavity pressure resists further deflection of the diaphragm. The relative change in the reference pressure due to the deflection of the diaphragm is given by [21]

$$\frac{\Delta p_{ref}}{p_{ref}} = \frac{1}{1 - \frac{\Delta V}{V}} - 1, \tag{5}$$

where Δp_{ref} is the change in reference pressure p_{ref} due to change in volume ΔV caused by the deflection of the diaphragm and V is the initial volume of the diaphragm. The larger the initial volume V of the diaphragm, the smaller is the change in reference pressure Δp_{ref} due to the deflection of the diaphragm. For practical

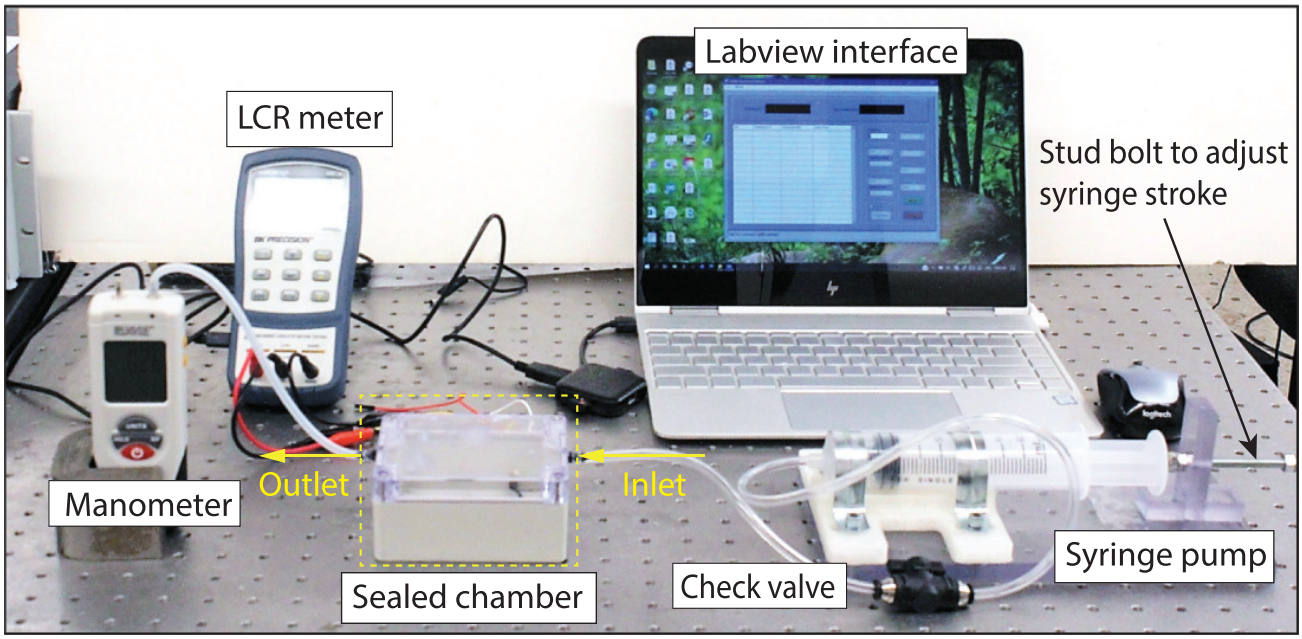

(a)

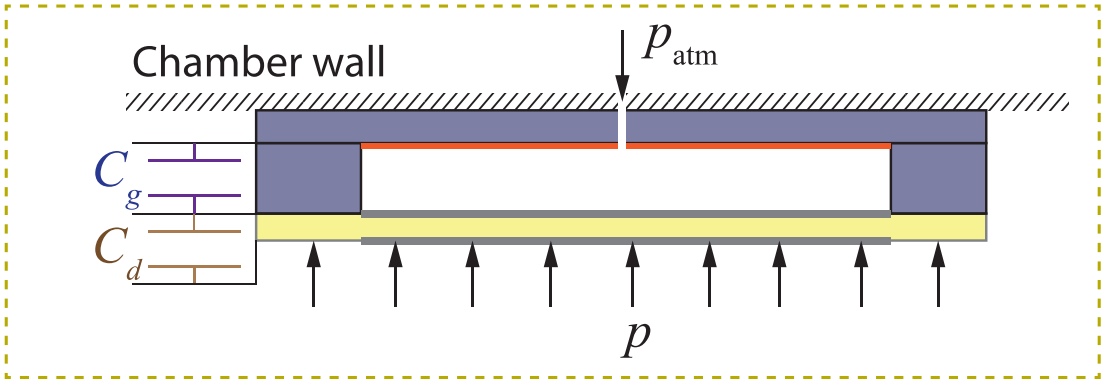

(b)

Figure 5: Pressure chamber experimental setup: (a) photograph of the experimental setup and (b) cross-sectional illustration of the capacitive pressure sensor in the sealed chamber under open cavity conditions. The color scheme of the materials corresponds to the same scheme shown in Figure 4.

applications, to ensure that the measurement error due to this change in reference pressure remains below 1%, V should be at least 100 times greater than ΔV [21]. The airfoil to which this sensor is integrated should thus be provided with features to exploit the high sensitivity of the open cavity pressure sensor for high resolution wind speed measurements. However, it should also be noted that the sensor exhibits better linearity when the cavity is sealed compared to its open cavity performance. Therefore, by adjusting the reference pressure, the linearity of the sensor can be adjusted, but at the cost of reduced sensitivity.

Table 3 summarizes the measured sensitivity and nonlinearity of the dual layer capacitive pressure under sealed and open cavity conditions based on Figure 6. It can be observed that under open cavity condition, the air gap capacitance C_g exhibits an overall sensitivity of 5.28 fF Pa^{-1}, calculated based on the line of best fit (LBF), which is about 35.2 times larger than the sensitivity for the sealed cavity condition. It should also be noted that under open cavity conditions, the air gap capacitance exhibits different LBF sensitivities for positive and negative pressures and high nonlinearity compared to the diaphragm capacitor within the investigated pressure

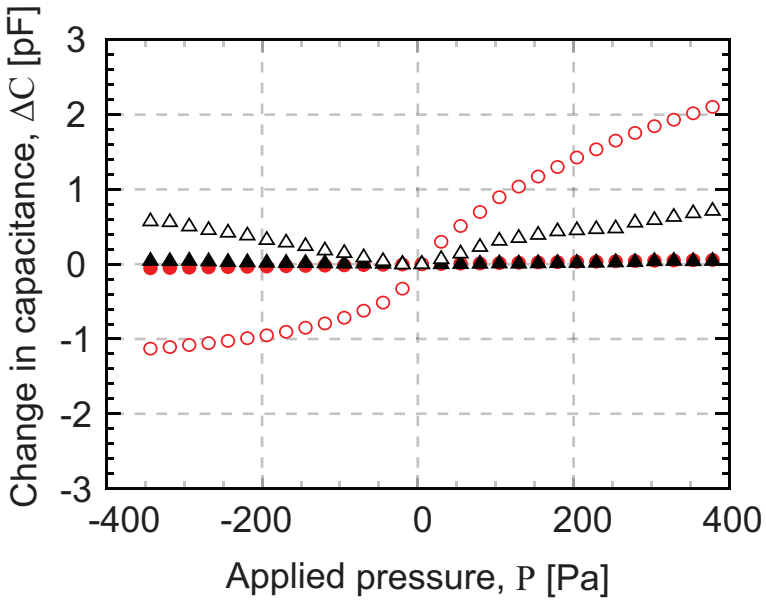

Figure 6: Mean changes in air gap capacitance (circles) and diaphragm capacitance (triangles) vs applied pressure under sealed (solid markers) and open (open markers) cavity conditions.

range. Since the thickness of the diaphragm layer reduces irrespective of the direction of the applied pressure, in spite of its linear characteristics, it should be used in conjunction with the air gap capacitor to distinguish between positive and negative pressures. Further, it is noticed that the diaphragm capacitor exhibited non-monotonic behavior for the sealed cavity, which is suspected to be due to the low signal-to-noise ratio. Nevertheless, the diaphragm configuration offers design freedom to increase pressure sensitivity by using a high dielectric constant material, such as P(VDF-TrFE-CTFE) as the deflecting layer, which has similar elastic compliance but with a dielectric constant five times higher than PVDF.

After characterization, the capacitive sensor is integrated into an airfoil having a NACA-2412 profile. A commercial 3D magnetometer module (Adafruit LSM303AGR) is also mounted within the airfoil for direction measurements. This completed airfoil anemometer is mounted on a rod on which it is free to rotate, and placed in a laboratory wind tunnel (Pitsco X-Stream) for demonstration, as shown in 7. As expected, the capacitance of the capacitive sensor increased quadratically with an increase in wind speed and the magnetometer successfully output the orientation of the airfoil.

Table 3: Measured sensitivities and coefficient of determination (R^2) of the dual layer capacitive sensor under sealed and open cavity conditions.

Cavity conditions	Pressure type	Air gap capacitor		Diaphragm capacitor	
		LBF sensitivity [fF Pa^{-1}]	R^2 [%]	LBF sensitivity [fF Pa^{-1}]	R^2 [%]
Sealed	Negative	0.15	99.8	0.13	95.7
	Positive	0.15	99.8	0.12	93.4
	Overall	0.15	99.8	0.11	97.8
Open	Negative	2.72	84.8	1.89	99.5
	Positive	5.48	97.1	1.79	95.8
	Overall	5.28	95.3	1.88	99.3

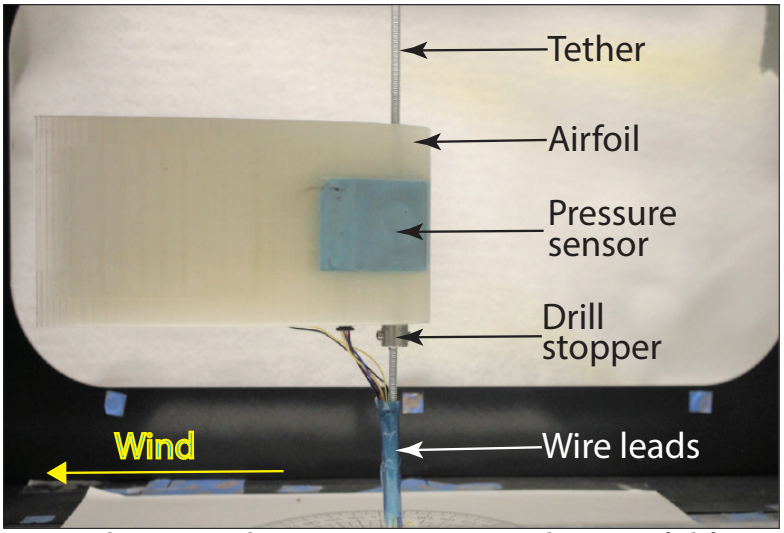

Figure 7: Capacitive sensor and commercial magentometer integrated in an airfoil for testing in a wind tunnel.

6. CONCLUDING REMARKS

An airfoil anemometer is presented and demonstrated for wind speed and direction measurement on tethered airborne applications. The selected NACA-2412 airfoil contour reduces the aerodynamic drag of the tether while aligning with the wind for direction measurement via an embedded commercial magnetometer. The airfoil also houses a flush-mounted diaphragm-type capacitive sensor which was developed as an alternative to conventional wind speed measurement technologies which exhibit disadvantages such as high aerodynamic drag or high power consumption. Details were presented for fabrication of the capacitive sensor from PVDF and Mylar sheet material, which was then characterized in a pressure chamber. For both the air gap and diaphragm capacitors, the open cavity provided an order of magnitude higher sensitivity than the sealed cavity. However, increasing the volume of the sealed cavity without changing the air gap would allow for the sensitivity to be increased. While the air gap capacitor was less linear than the diaphragm capacitor, it provided a 2.8 times higher overall sensitivity at 5.28 fF Pa^{-1} for the open cavity, while also making it possible to distinguish between positive and negative pressures. Future modeling of the sensor capacitance will enable the sensor to be designed for airfoil anemometers over a targeted range of wind speed.

ACKNOWLEDGMENTS

Financial support was provided by the member organizations of the Smart Vehicle Concepts Center, a Phase III National Science Foundation Industry-University Cooperative Research Center (www.SmartVehicleCenter.org) under grant NSF IIP 1738723.

References

[1] Lackner, M., Rogers, A., and Manwell, J., "Uncertainty analysis in wind resource assessment and wind energy production estimation," in [*45th AIAA Aerospace Sciences Meeting and Exhibit*], 1222 (2007).

[2] Wang, J., Ding, W., Pan, L., Wu, C., Yu, H., Yang, L., Liao, R., and Wang, Z., "Self-powered wind sensor system for detecting wind speed and direction based on a triboelectric nanogenerator," *ACS Nano* **12**(4), 3954–3963 (2018).

[3] Sanz-Andrés, Á., Pindado, S., and Sorribes-Palmer, F., "Mathematical analysis of the effect of rotor geometry on cup anemometer response," *The Scientific World Journal* **2014** (2014).

[4] Gao, S., Yi, Z., Ye, Y., Qin, M., and Huang, Q., "Temperature effect and its compensation of a micromachined 2-D anemometer," *IEEE Sensors Journal* **19**(14), 5454–5459 (2019).

[5] Matova, S., Makinwa, K., and Huijsing, J., "Compensation of packaging asymmetry in a 2-D wind sensor," *IEEE Sensors Journal* **3**(6), 761–765 (2003).

[6] Foss, J., Peabody, J., Norconk, M., and Lawrenz, A., "Ambient temperature and free stream turbulence effects on the thermal transient anemometer," *Measurement Science and Technology* **17**(9), 2519 (2006).

[7] Han, D., Kim, S., and Park, S., "Two-dimensional ultrasonic anemometer using the directivity angle of an ultrasonic sensor," *Microelectronics Journal* **39**(10), 1195–1199 (2008).

[8] Ghahramani, A., Zhu, M., Przybyla, R., Andersen, M., Galicia, P., Peffer, T., Zhang, H., and Arens, E., "Measuring air speed with a low-power mems ultrasonic anemometer via adaptive phase tracking," *IEEE Sensors Journal* **19**(18), 8136–8145 (2019).

[9] Bian, Y., Liu, R., Huang, X., Hong, J., Huang, H., and Hui, S., "Design and fabrication of a metal core PVDF fiber for an air flow sensor," *Smart Materials and Structures* **24**(10), 105001 (2015).

[10] Al-Rubaiai, M., Tsuruta, R., Gandhi, U., Wang, C., and Tan, X., "A 3D-printed stretchable strain sensor for wind sensing," *Smart Materials and Structures* **28**(8), 084001 (2019).

[11] Cho, L., Lu, C., Zhang, A., and Tam, H., "Fiber bragg grating anemometer with reduced pump power-dependency," *IEEE Photonics Technology Letters* **25**(24), 2450–2453 (2013).

[12] Adel, M., "A comparative study for different shapes of airfoils," *International Journal of Mechanical Engineering* **4** (2019).

[13] "Center of pressure." https://www.grc.nasa.gov/www/k-12/airplane/cp.html. Accessed: 2021-05-02.

[14] Wekesa, D., Mutuku, J., and Kamau, J., "Microcontroller-based data logging instrumentation system for wind speed and direction measurements," *Journal of Agriculture, Science and Technology* **14**(1) (2012).

[15] Camuffo, D. and Denegri, A., "A method for measurement of mean wind direction with the use of standard potentiometric transducers," *Atmospheric Environment (1967)* **10**(5), 415 (1976).

[16] Moafipoor, S., Grejner-Brzezinska, D., and Toth, C., "Adaptive calibration of a magnetometer compass for a personal navigation system," in [*IGNSS Symposium*], (2007).

[17] Abbott, I. and Von Doenhoff, A., [*Theory of wing sections: including a summary of airfoil data*], Courier Corporation (2012).

[18] Wang, J., Geng, L., Ding, L., Zhu, H., and Yurchenko, D., "The state-of-the-art review on energy harvesting from flow-induced vibrations," *Applied Energy* **267**, 114902 (2020).

[19] Laflamme, S., Saleem, H., Vasan, B., Geiger, R., Chen, D., Kessler, M., and Rajan, K., "Soft elastomeric capacitor network for strain sensing over large surfaces," *IEEE/ASME Transactions on Mechatronics* **18**(6), 1647–1654 (2013).

[20] An, L., Lu, T., Xu, J., Wang, Z., Xu, M., and Wang, T., "Soft sensor for measuring wind pressure," *International Journal of Mechanical Sciences* **141**, 386–392 (2018).

[21] Xiong, W., Guo, D., Yang, Z., Zhu, C., and Huang, Y., "Conformable, programmable and step-linear sensor array for large-range wind pressure measurement on curved surface," *Science China Technological Sciences* **63**(10), 2073–2081 (2020).

[22] Hu, X. and Yang, W., "Planar capacitive sensors–designs and applications," *Sensor Review* (2010).

[23] Shi, T., Xie, C., Huang, S., Williams, R. A., and Beck, M., "Capacitance-based instrumentation for multi-interface level measurement," *Measurement Science and Technology* **2**(10), 923 (1991).

[24] Igreja, R. and Dias, C., "Analytical evaluation of the interdigital electrodes capacitance for a multi-layered structure," *Sensors and Actuators A: Physical* **112**(2-3), 291–301 (2004).

[25] Chen, Z. and Luo, R., "Design and implementation of capacitive proximity sensor using microelectromechanical systems technology," *IEEE Transactions on Industrial Electronics* **45**(6), 886–894 (1998).

[26] Inui, T., Koga, H., Nogi, M., Komoda, N., and Suganuma, K., "A miniaturized flexible antenna printed on a high dielectric constant nanopaper composite," *Advanced Materials* **27**(6), 1112–1116 (2015).